Inward-facing conformation of glutamate transporters as revealed by their inverted-topology structural repeats

Thomas J. Crisman[a,1], Shaogang Qu[b,1], Baruch I. Kanner[b], and Lucy R. Forrest[a,2]

[a]Computational Structural Biology Group, The Max Planck Institute of Biophysics, Max-von-Laue-Strasse 3, 60438 Frankfurt am Main, Germany; and [b]Department of Biochemistry, Hadassah Medical School, Hebrew University, 91220 Jerusalem, Israel

Edited by Christopher Miller, Brandeis University, Waltham, MA, and approved October 16, 2009 (received for review July 31, 2009)

Glutamate transporters regulate synaptic concentrations of this neurotransmitter by coupling its flux to that of sodium and other cations. Available crystal structures of an archeal homologue of these transporters, GltPh, resemble an extracellular-facing state, in which the bound substrate is occluded only by a small helical hairpin segment called HP2. However, a pathway to the cytoplasmic side of the membrane is not clearly apparent. We previously modeled an alternate state of a transporter from the neurotransmitter:sodium symporter family, which has an entirely different fold, solely on the presence of inverted-topology structural repeats. In GltPh, we identified two distinct sets of inverted-topology repeats and used these repeats to model an inward-facing conformation of the protein. To test this model, we introduced pairs of cysteines into the neuronal glutamate transporter EAAC1, at positions that are >27 Å apart in the crystal structures of GltPh, but ≈10 Å apart in the inward-facing model. Transport by these mutants was activated by pretreatment with the reducing agent dithithreitol. Subsequent treatment with the oxidizing agent copper(II)(1,10-phenantroline)$_3$ abolished this activation. The inhibition of transport was potentiated under conditions thought to promote the inward-facing conformation of the transporter. By contrast, the inhibition was reduced in the presence of the nontransportable substrate analogue D,L-threo-β-benzyloxyaspartate, which favors the outward-facing conformation. Other conformation-sensitive accessibility measurements are also accommodated by our inward-facing model. These results suggest that the inclusion of inverted-topology repeats in transporters may provide a general solution to the requirement for two symmetry-related states in a single protein.

alternating access | conformationally sensitive cross-linking | homology modeling | neurotransmitter | secondary transport

Glutamate is a ubiquitous signaling molecule in excitatory neuronal synapses. However, for efficient neurotransmission, and to avoid neurotoxicity, the concentration of glutamate in the synapse is carefully regulated through reuptake into the neuronal and glial cells surrounding the synapse. The proteins responsible for this uptake, the so-called excitatory amino acid transporters (EAATs), are capable of accumulating glutamate against a concentration gradient of up to 10^6 (1, 2). EAATs accomplish this by coupling glutamate transport to the passive diffusion of cations, first by cotransport of sodium and protons (1, 2), and subsequently by countertransport of potassium (3–5) (Fig. 1).

In recent years, crystallographic studies have revealed the atomic-resolution structures of several secondary transporter families. In the case of the EAATs, the structure of a bacterial aspartate transporter GltPh from *Pyrococcus horokoshii* (6, 7) has provided key insights into various aspects of transport, in strong agreement with biochemical, electrophysiological, and other experimental data (8). The GltPh structure contains eight transmembrane (TM) helices, as well as two helix-turn-helix motifs, HP1 and HP2, which point toward the center of the membrane from opposite sides. The substrate and ion binding sites are located close to the point where the tips of HP1 and HP2 meet. The available structures of GltPh, which vary in substrate or inhibitor occupancy, all correspond to a conformation resembling an outward-facing state, where the substrate binding site is essentially exposed to the extracellular solution (6, 7). Specifically, the substrate can become occluded by the closure of HP2, like a flap, whereas the pathway to the cytoplasm is blocked by ≈20 Å of packed protein. However, transport is generally believed to involve a mechanism in which the central binding site for substrate becomes alternately accessible to one side or the other of the membrane during the transport cycle (9). Here, we attempt to model the alternate, inward-facing form of the transporter using the presence of internal inverted-topology repeats in the structure.

We previously generated an atomistic model of an inward-facing conformation of an NSS transporter, LeuT, which contains an inverted-topology repeat of five TM helices, by swapping the conformation of the repeats in the outward-facing x-ray structure. That is, threading the sequences of the first five TM helices onto the structure of the second five TM helices, and vice versa, revealed a model in which the central binding site was accessible to the cytoplasm and closed to the outside. The change in conformation occurs because the five TM repeats in LeuT, although clearly related, are not identical in structure (10). Moreover, the small differences between them appear to be responsible for the structure adopting an extracellular-facing conformation in the x-ray structure. The cytoplasmic pathway revealed in the swapped model was in very good agreement with cysteine-scanning mutagenesis and accessibility measurements, as well as with the pathway of a related protein, vSGLT, for which a structure was subsequently reported in an inward-facing orientation (11). Consequently, we have proposed that such inverted-topology repeats might be an integral feature of transporters (10).

In the present study, we show that inverted repeats in GltPh structures can be used to model an alternate conformation of EAATs in which the substrate binding site is exposed to the cytoplasm. The large conformational change predicted by this model is supported by conformation-dependent cross-linking of site-directed cysteine mutants of a mammalian glutamate transporter, EAAC1. The model is also in harmony with conformation-dependent accessibility of engineered cysteines to the membrane-permeant sulfhydryl reagent *N*-ethyl maleimide (NEM) (12).

Author contributions: B.I.K. and L.R.F. designed research; T.J.C., S.Q., and L.R.F. performed research; B.I.K. and L.R.F. analyzed data; and B.I.K. and L.R.F. wrote the paper.

The authors declare no conflict of interest.

This article is a PNAS Direct Submission.

Data deposition: The trimer models have been deposited in the Protein Model Database, http://mi.caspur.it/PMDB [PMDB ID codes PM0075966 (2NWL-based model) and PM0075968 (2NWW-based model)].

[1]T.J.C. and S.Q. contributed equally to this work.

[2]To whom correspondence should be addressed. E-mail: lucy.forrest@biophys.mpg.de.

This article contains supporting information online at www.pnas.org/cgi/content/full/0908570106/DCSupplemental.

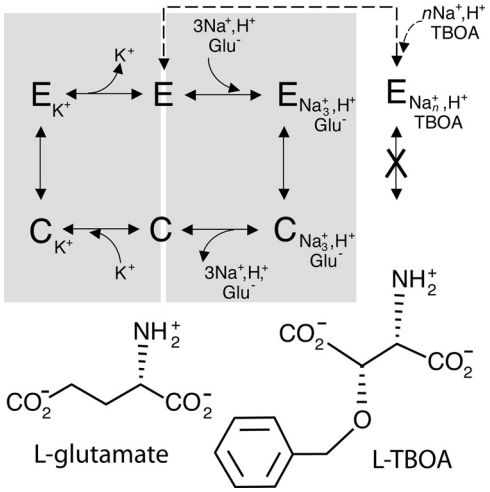

Fig. 1. Transport by the mammalian EAATs. The transport cycle of mammalian EAATs involves two half-cycles (gray boxes). First, sodium, protons, and glutamate from the extracellular medium bind to an extracellular-facing conformation of the protein (E). A subsequent conformation change to form a cytoplasm-facing conformation (C) allows access to the binding site from the cytoplasm so that the substrates can be released. In the second half-cycle, intracellular potassium binds, the protein returns to an extracellular-facing conformation, and potassium can be released to the extracellular medium. Thus, addition of potassium to the extracellular solution increases the proportion of transporters in an inward-facing conformation. Transport can be interrupted by binding of nontransportable glutamate analogues (TBOA) with sodium, locking the protein in an outward-facing conformation.

Results

Structure of GltPh Contains Inverted-Topology Structural Repeats. Previous analysis of the structure of GltPh suggested a structural relationship between the two hairpin loops and half of their adjacent helices (6). This relationship can be extended to include the entirety of TM7 and TM8, albeit with reduced structural similarity [supporting information (SI) Table S1 and Fig. 2*A*; see also *SI Materials and Methods*]. The resultant structural alignment provides better coverage of the protein structure, which is important for the modeling. These segments have opposite topologies in the membrane, and therefore one of them has to be rotated by ≈180° around an axis in the plane of the membrane to achieve the fit.

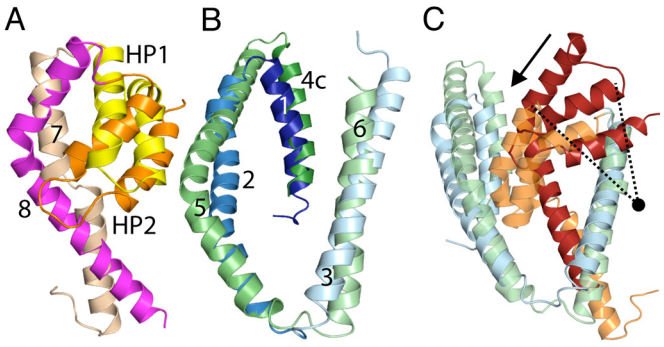

Fig. 2. Structural similarity and differences between segments of GltPh. Structural alignments of (*A*) HP1 (yellow) plus TM7 (pale orange), against HP2 (orange) plus TM8 (magenta), and (*B*) TM 1 to 3 (shades of blue) with TM 4c to 6 (shades of green). In (*C*) we considered TM 1 to 3 (blue), plus HP2 and TM8 (*red*) as one pseudorepeat, and TM 4c-6 (green), HP1 and TM7 (orange) as a second repeat. Note that only the first three TMs were used for the fit: this structural superposition highlights the shift in position of the hairpin-TM motif with respect to the first three TMs of each pseudorepeat (arrow), which is a vertical curving movement (the approximate pivot point is shown as a circle). Figures were made using PyMOL (33).

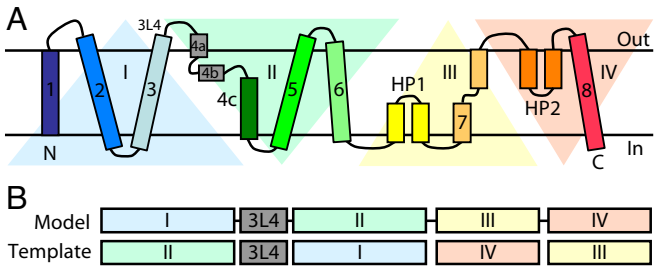

Fig. 3. Organization of repeats in GltPh. (*A*) Schematic of the topology of GltPh emphasizing the structural relationships between the four segments, I to IV. (*B*) Schematic of the sequence alignment used to generate the swapped-repeat model. For example, segment I was modeled using the structure of segment II as a template. The conformation of the loop between TMs 3 and 4 (3L4) was taken from the x-ray structure.

We also investigated the six TM helices in the N-terminal half of GltPh, which comprise the so-called "cylinder." This region has recently been suggested to contain a repeat of two TM helices (13). By including helix 4c (which spans the membrane), but excluding helices 4a and 4b (which do not span the membrane), we obtained a reasonable structural alignment between two 3-TM domains in this N-terminal cylinder (see Table S1 and Fig. 2*B*). The decision to exclude helices 4a and 4b (and the 3–4 loop) from the repeat is consistent with the large sequence insertion in this region in human EAAT homologues.

Based on the above analysis, the structure of GltPh can be described as containing four inverted-topology segments (which we refer to as I to IV) (Fig. 3*A*). That is, there is a pseudo 2-fold symmetry relationship between segments I and II, and another between segments III and IV.

In LeuT we observed a break in the symmetry between the five TM repeats, which was responsible for the formation of an asymmetric structure of the whole protein (10). In GltPh, by treating segments I and IV as one structural unit, and segments II and III as a second structural unit, and by superposing only segment I on segment II, we noticed a large difference in the position of the second half of each unit relative to the first half (Fig. 2*C*). Because the trimeric interface involving TMs 2, 4, and 5 is known to be unchanged during transport (14), we assume that any conformational changes within a given protomer would most likely involve segments III and IV rather than segments I and II. Consequently, it appears from Fig. 2*C* that the position of segment III is significantly lower within the membrane than the position of segment IV with respect to segments I or II.

Swapping the Conformations of Inverted Repeats Reveals a Cytoplasmic Facing Structure. We used the presence of inverted-topology repeats in GltPh to model an alternate conformation of GltPh using the approach used for the NSS proteins, namely swapping of the conformations of the repeats (10). Because there are four repeat segments in GltPh rather than two, as in LeuT, we adjusted the protocol slightly. Thus, the conformation of segment I was modeled using the structure of repeat II as a template, and vice versa, while the conformation of segment III was modeled on IV, and vice versa (Figs. S1*A* and S2 and Fig. 3*B*).

The model of GltPh generated by swapping the conformations of the repeats contains a large conformational change with respect to the crystal structure, and appears to represent the cytoplasm-facing state of the protein (Fig. S1 *C* and *D* and Fig. 4*A*). Because the helices forming the subunit interface in the trimer (particularly TMs 4a, 4b, 4c, and 5) are likely to be fixed, according to evidence from cysteine cross-linking (14), we discuss the changes in the rest of the protein with respect to these helices. The major difference that can be observed is that the

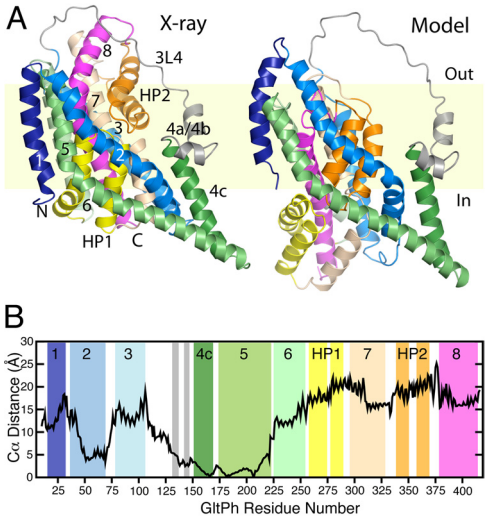

Fig. 4. Model of GltPh in a cytoplasm-facing conformation. (*A*) Structure of a protomer of the cytoplasm-facing model (*Right*) compared with the x-ray crystal structure of the extracellular-facing conformation (*Left*). The protein is viewed along the plane of the membrane, with the extracellular side at the top, and colored as in Fig. 3. (*B*) Distance between Cα atoms in the outward-facing structure and the model of the inward-facing conformation. For this calculation, the structures were superposed using TMs 4c and 5 (residues 151–218) at the subunit interface, which is believed not to change during transport (14).

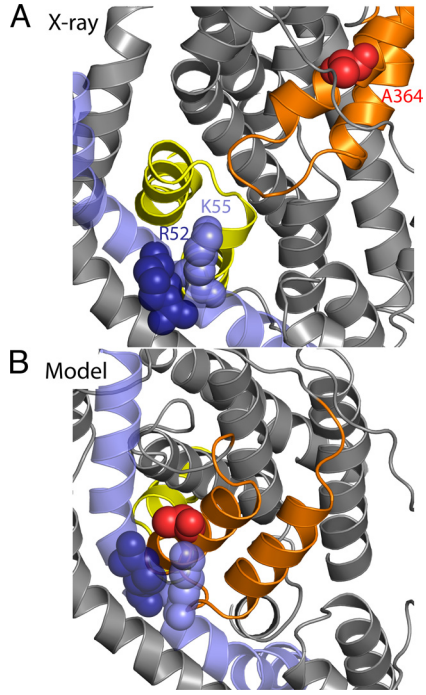

Fig. 5. Cross-linking residues become close in the cytoplasm-facing model of GltPh. Residues R52 (dark blue spheres), K55 (blue spheres), and A364 (red spheres) from TM2 (blue) and HP2 (orange) are shown in the x-ray structure (*A*) and in the cytoplasm-facing model (*B*). These residues correspond, respectively, to R61C, K64C, and V420C of EAAC1.

core of the protein containing the binding site is predicted to have moved toward the cytoplasm by 15 to 25 Å relative to the subunit interface (see Fig. 4 *A* and *B*). As a consequence, HP1 becomes exposed to the cytoplasmic solution, analogous to the extracellular exposure of HP2 in the x-ray structure (see Fig. S3 and Fig. 4*A*). This exposure of HP1 provides a means for release of substrate into the cytoplasm, namely by the flapping open of HP1, as has been suggested for HP2 in the extracellular conformation (7). In addition, the model predicts that HP2 will become buried under TMs 2 and 5 (see Fig. S3 and Fig. 4*A*), so that release of substrate and ions back to the extracellular environment would be inhibited significantly.

The model also suggests changes of 15 to 20 Å in the positions of TMs 7 and 8 to accompany the movements of HP1 and HP2 (see Fig. 4*B*). Such a concomitant movement may enable the binding site formed between these helices to be maintained. TMs 3 and 6, which shield TMs 7 and 8 from the lipid, are also shifted in the same direction, although to a lesser extent (10–15 Å). TM1 also moves somewhat, but in the opposite direction: that is, upwards in the membrane. In summary, the model predicts that the protein core consisting of HP1, TM7, HP2, and TM8 moves inward relative to the rest of the protein to form a cytoplasm-facing conformation that may correspond to an alternate state in the transport cycle.

Cysteine Cross-Linking Supports Close Approach of TM2 and HP2. The large movements suggested by this model are supported by evidence for cysteine cross-linking in EAAT1 (15). Specifically, mutations to cysteine at positions equivalent to GltPh residues 52 or 55 (from TM2) and 364 (from HP2b) were found to cross-link in EAAT1, resulting in a loss of transporter activity (15). The Cα atoms of these residues are 27 to 29 Å apart in the x-ray structure of GltPh, and thus it is unlikely that they cross-link in this state (Fig. 5*A*). By contrast, in our model, TM2 has a significant interface with HP2. The distance between the Cα atoms in these cysteine pairs is ≈10 Å, which is significantly closer to the 7 to 8 Å expected for disulfide formation (see Fig. 5*B*). To test whether the cross-linking of HP2b and TM2 has a higher probability under conditions in which the transporter becomes inward-facing, we analyzed the equivalent double-cysteine mutants of EAAC1 (also known as EAAT3), with cysteines introduced at V420 of HP2, and at either R61 or K64 of TM2.

Aspartate transport by either R61C/V420C or K64C/V420C was stimulated by 50 to 70% upon addition of the reducing agent dithiothreitol (DTT) (Fig. 6 *A* and *B*), suggesting that the cysteine pairs spontaneously cross-link, similar to the observations for EAAT1 (15). Such cross-linking often inhibits transport (16–18), presumably because the disulfide imposes restrictions on the protein conformational changes necessary for transport, although such inhibition may also be the result of steric hindrance or another distortion introduced by the cross-link. Preincubation with 30 or 100 μM of the oxidizing agent copper (II)(1,10-phenantroline)$_3$ (CuPh) resulted only in modest inhibition of transport, supportive of the notion that many of the cysteine pairs are already cross-linked. An almost full inhibition of transport was observed when the CuPh concentration was increased to 300 μM (see Fig. 6 *A* and *B*). Upon prior activation by DTT, the activity of the newly reduced transporters was fully sensitive to CuPh (see Fig. 6 *A* and *B*).

These results indicate that when cross-linking is complete, all transporters are locked permanently in one conformation so that the translocation cycle is blocked. Thus, when transport is measured subsequent to exposure to lower concentrations of CuPh (such as 100 μM used in the experiment depicted in Fig. 7), the remaining activity is a read-out of the proportion of those transporters that were not yet cross-linked.

The effects of DTT and CuPh on transport were only observed for the double-cysteine mutants, and not for the equivalent single-cysteine mutants (V420C, R61C, or K64C) expressed either alone or together: for example, V420C with R61C or with K64C (Fig. 6*C*). These results suggest that both cysteines need to be present on the same polypeptide chain for cross-linking to

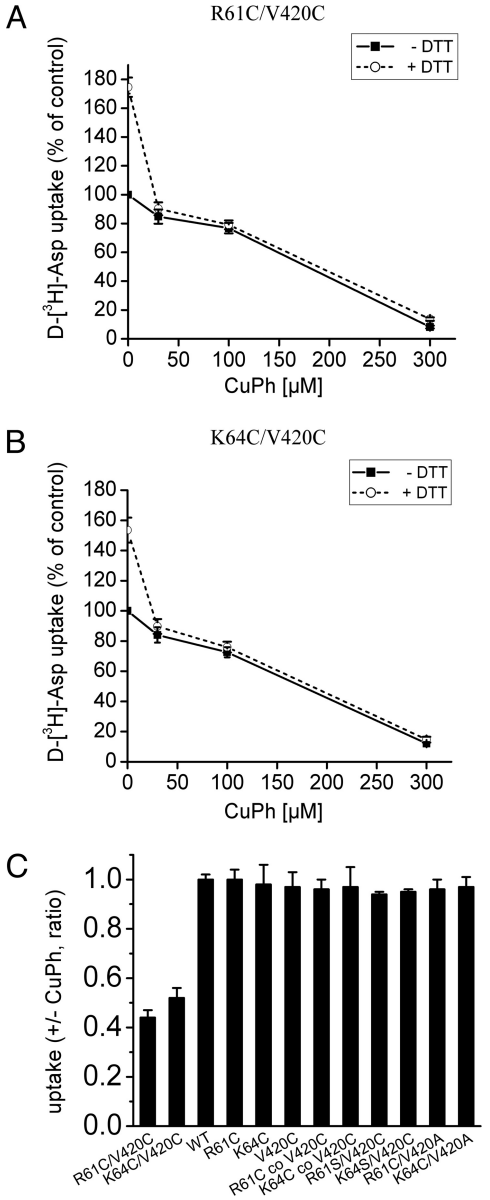

Fig. 6. Effect of DTT and CuPh on D-[^{3}H]aspartate transport by R61C/V420C and K64C/V420C. Transport of D-[^{3}H]aspartate was measured in *Xenopus laevis* oocytes expressing the indicated mutants after pretreatment for 5 min in the presence or absence of 5-mM DTT, followed by a 5-min incubation with CuPh, as described in *Materials and Methods*. (*A* and *B*) Initial treatment in the presence or absence of 5-mM DTT was followed by a 5-min incubation with the indicated concentrations of CuPh. Results are expressed as percent of activity of oocytes that were preincubated twice for 5 min in frog Ringer's solution without DTT or CuPh. (*C*) After preincubation with DTT, the oocytes were incubated for 5 min in the presence or absence of 100-μM CuPh. The results are expressed as the ratio of uptake in the presence of CuPh over that in its absence. ''R61C co V420C'' and ''K64C co V420C'' represent oocytes in which the two indicated cRNAs were coinjected.

occur. Moreover, no effect of CuPh or DTT was seen with single-cysteine mutants in which the other residue was converted to either Ser or Ala, namely R61S/V420C, K64S/V420C, R61C/V420A, or K64C/V420A (see Fig. 6*C*). Thus, it seems unlikely that inhibition occurs as a result of cross-linking of one of the introduced cysteines to an endogenous cysteine.

Cysteine Cross-Linking Can Be Modulated by Substrate and Inhibitors. To determine the effect of the conformation of the transporter on the rate of cross-linking, the initial activation of the double-

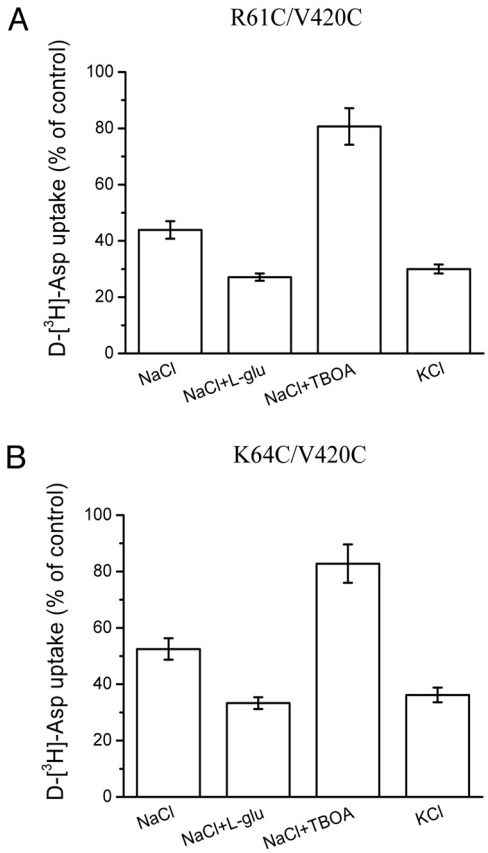

Fig. 7. Effect of the medium composition during CuPh treatment on the transport activity of R61C/V420C and K64C/V420C. Oocytes expressing R61C/V420C (*A*) or K64C/V420C (*B*) were pretreated with 5-mM DTT for 5 min, followed by incubation for 5 min with 100-μM CuPh in either: frog Ringer's solution in the absence or presence of either 1-mM L-glutamate or 60 μM of TBOA or frog Ringer's solution in which all of the NaCl was replaced by KCl. The results are expressed as a percentage of activity of oocytes incubated without CuPh.

cysteine mutants by DTT was followed by incubation for 5 min with 100-μM CuPh under various conditions. Transport was subsequently measured after washing out the CuPh. When the sodium-containing medium was either supplemented with glutamate or replaced by potassium, conditions that promote the formation of the inward-facing conformation (see Fig. 1), the inhibition by 100 μM CuPh was potentiated (see Fig. 7). This suggests that the cysteine residues are indeed closer together in the inward-facing conformation. By contrast, addition of the nontransportable substrate analogue D,L-threo-β-benzyloxyaspartate (TBOA) reduced the cross-linking effect of CuPh (see Fig. 7), consistent with the expectation that TBOA increases the proportion of protein trapped in an outward-facing conformation in which the cysteines are far apart. In the absence of external sodium (replacement with choline) there was very little impact, if any, of glutamate or TBOA (Fig. S4), apparently because glutamate translocation and TBOA binding both require sodium (see Fig. 1).

In principle, the modulation of the inhibition by CuPh could be a result of changes in accessibility of the engineered cysteine residues, rather than in their distance. As a measure of their aqueous accessibility, we determined the effect of MTS reagents on transport by the single cysteine mutants, although it is true that these reagents are larger than the reactive oxygen species generated by CuPh. Preincubation of R61C or K64C with MTSES (2-sulphonatoethyl-methanethiosulfonate) resulted in inhibition of transport, which was potentiated by either glutamate or external

potassium (Fig. S5). However, TBOA, which protected against cross-linking of the cysteine pairs (see Fig. 7), did not modulate the inhibition of R61C or K64C by MTSES (see Fig. S5). For V420C, inhibition of transport by MTSET [(2-trimethylammonium) methanethiosulfonate] was protected not only by TBOA but also by glutamate (see Fig. S5), which again is different from the cross-linking results. Thus, while the accessibility of the introduced cysteines to MTS reagents appears to be dependent on the conformational state of the transporter, the effects of substrates and substrate analogues on cross-linking cannot be explained merely in terms of such changes in accessibility.

Discussion

Experimental Evidence in Support of the Cytoplasm-Facing Model. Available x-ray crystal structures of GltPh bound to either the substrate aspartate, or to a nontransportable analogue TBOA, have similar conformations (6, 7). Both are essentially outward-facing, although in the absence of TBOA the helix-turn-helix segment HP2 provides a thin barrier that appears to flap open to expose the substrate binding site to the extracellular solution (see Fig. 4*A*) (13). To date, proposed mechanisms of the conformational change required to expose this aspartate binding site to the cytoplasmic solution have invoked relatively small movements in the protein, involving mainly HP1, with the rest of the structure remaining essentially unchanged (6, 7, 19). Our atomistic model suggests that the cytoplasm-facing conformation of GltPh is a symmetry-related version of the extracellular-facing structures, and that the inward- and outward-facing states interchange through a large, concerted movement of the core binding region of HP1, TM7, HP2, and TM8 (see Figs. 4 and 5).

The prediction of a large conformational change in the EAATs is supported by the observation that HP2 and TM2 can spontaneously cross-link in both EAAC1 (see Fig. 6) and EAAT1 (15), even though the equivalent residues are >27 Å apart in the x-ray structures (see Fig. 5*A*), much too far to allow formation of a disulfide bond. Our model predicts a marked reduction of this distance to ≈10 Å. Furthermore, the fact that oxidative cross-linking is potentiated under conditions with increased proportions of inward-facing transporters, and reduced when the fraction of outward-facing transporters is increased (see Figs. 1 and 7), supports the idea that HP2 and TM2 indeed become closer in the cytoplasm-facing conformation of the transporter.

Large conformational changes are also supported by kinetic analysis of EAAC1, which showed that glutamate translocation is associated with energetic barriers of ≈100 kJ/mol (20). By contrast, distance measurements in EAAT3 using FRET suggest very little structural change in the protein (21). However, if the inward-facing states are relatively short-lived, then the latter measurements may not report on them, because FRET measures an average signal over all states.

Our model also predicts significant changes in solvent accessibility, so that most of HP1 and the cytoplasmic halves of TM7 and TM8 are accessible to intracellular solution in the model (Fig. S6 *B* and *E*), whereas they are buried within TMs 2, 3, 5, and 6 in the x-ray structure (Fig. S6 *A* and *D*). This prediction is consistent with the reactivity to NEM of cysteine residues introduced into these regions of a related transporter GLT-1/EAAT2 (12); this reactivity increases in the presence of extracellular potassium. We were able to match calculated and measured accessibility of many, but not all, of the residues in this region for the model based on Asp-bound GltPh (see Fig. S6 *B* and *E*). Closer agreement, particularly for residues in HP1, was observed for a second model in which HP1 is more open (Fig. S6 *C* and *F*). Disagreement between measured and calculated accessibility at a few positions may reflect inaccuracies in the models, such as slight rotational or translational errors in helix position, which can affect the calculated accessibility of individual residues. Differences between GLT-1 and GltPh may also affect the comparison. Nevertheless, the overall trend in these data (i.e., that these segments become more accessible in inward-facing conformations) is very consistent with the proposed model (see Fig. S6).

Analogous cysteine-accessibility measurements for HP2 of GLT-1 revealed that substrates and inhibitors have complex effects on their reactivity to the cysteine modifier MTSET (22). Some residues, such as 448 and 449 (GLT-1 numbering), are protected from reacting with MTSET in the presence of glutamate, consistent with being buried under TM2 in the inward-facing model (see Fig. 4*A*), as well as with a likely reduction in mobility of HP2. However, several of the reactive residues in HP2 of GLT-1 are also protected by the nontransportable substrate analogue kainate (22), even though kainate likely holds the protein in an outward-facing conformation. This apparent contradiction can be explained by an increase in contacts between HP2 and 3L4 (the loop between TMs 3 and 4) observed upon TBOA binding, which reduces the accessibility of residues in HP2 (7). Other residues in HP2 are, surprisingly, more accessible in the presence of TBOA than of kainate (22). Because some of these residues are on the underside of HP2, their accessibility may depend on the different degrees to which HP2 is wedged open by the two inhibitors.

Thus, the cysteine cross-linking, accessibility and other experimental data, are all consistent with the model of the inward-facing transporter. Clearly, however, ultimate proof of this prediction will require a crystal structure of a glutamate transporter trapped in this state.

A Mechanism of Alternating Access in EAATs. Based on our data, we propose a mechanism of alternating access in EAATs involving four major states of the transporter: two outward- and two inward-facing (Fig. S7). The first state is a substrate-free, outward-facing conformation (or ensemble thereof) in which HP2 is open, similar to TBOA-bound GltPh (7), as observed in molecular dynamics simulations (23, 24). Upon ion and substrate binding, HP2 would then close in to form an outward-facing, occluded state (see Fig. 4*A*).

In the next step, the core segment containing HP1, TM7, HP2, and TM8 would undergo the movement shown in Fig. 4 to form the inward-facing conformation of the model. This conformational change probably requires close packing of HP1 and HP2 against TMs 7 and 8, so that together they form a smooth sausage-shaped bundle. Thus, in acting as wedges that hold HP2 open, substrate analogues, such as TBOA, may inhibit their own transport by preventing this major conformational change. In the resultant inward-facing, occluded conformation, the thin intracellular gate would be formed by HP1. Release of substrates would then require opening of HP1 to form an inward-facing, open state, which has been modeled here based on the TBOA-bound structure (see Fig. S6*F*). This four-state mechanism is consistent with trypsin cleavage of GLT-1, which suggests that glutamate is bound to two major conformations of the protein, only one of which can be inhibited by the nontransportable analogue dihydrokainate (25). Finally, binding of intracellular potassium would then favor closure of HP1, facilitating the reverse conformational change to the outward-facing state.

A remarkable feature of the inward-facing model of GltPh is that it was constructed only based on the structures of the inverted-topology repeats inherent in the EAAT fold. An essential step in the modeling, therefore, was the identification of structural symmetry within the GltPh structure to cover as much of the structure as possible. In GltPh, one can think of segments I and IV as forming one single, noncontiguous pseudorepeat, while segments II and III form a second pseudorepeat with inverted topology to the first (see Fig. 3). We observed an asymmetry in those two pseudorepeats, so that segment III is

shifted vertically by ≈10 Å compared to segment IV (see Fig. 2*C*). This asymmetry reflects the location of the core protein segment (III and IV) within the cylinder (I and II), so that swapping the conformations of the repeats creates a vertical displacement of the whole III-IV segment, resulting in an inward-facing state.

Such observations not only provide a technique for predicting alternate conformations of transporters, but also give further support for the appealing idea of a role for inverted-topology repeats in the transport mechanism (10, 13). In such a mechanism, each repeat has the ability to adopt two distinct conformations with similar energies (10). Interchange between those conformations thus allows the formation of two different, but symmetry-related structures with analogous substrate pathways leading to opposite sides of the membrane, thereby elegantly solving the main requirements for alternating access.

Materials and Methods

Sequence Alignments. An initial sequence alignment between the model and template was obtained from structure and ClustalW sequence alignments (26) of the four segments (see Fig. S1 and Fig. 3), and was adjusted to optimize, for example, binding site positions (see Fig. S2 and *SI Materials and Methods*).

Construction of the Protomer Model. Models of GltPh protomers were built using Modeller 9v5 (27), where the template for each segment was the corresponding repeat from a GltPh crystal structure with PDB code 2NWL or 2NWW (see Fig. 3). Distance constraints were added to keep the internal conformations of certain local regions similar to the x-ray structure (see *SI Materials and Methods*). These distance constraints did not affect the overall conformational change predicted by the model.

Construction of Trimer Model. To construct trimeric models, we fitted the protomers onto the x-ray structure using helices TM3, 4a, 4b, TM4c, TM5, and TM6 (residues 82–253), and minimized changes at the protein-lipid interface (see *SI Materials and Methods*).

Generation and Subcloning of Mutants. The C-terminal his-tagged version of rabbit EAAC1 (28, 29) in the vector pBluescript SK^- (Stratagene) was used as a parent for site-directed mutagenesis (30, 31). This was followed by subcloning of the mutants into his-tagged EAAC1, residing in the oocyte expression vector pOG_1 (29) using unique restriction enzymes. The subcloned DNA fragments were sequenced between these unique restriction sites.

Expression of Transporters. Complementary DNAs encoding the his-tagged EAAC1 and its derived mutants, subcloned in pOG_1, were linearized with SacI, and cRNA was transcribed from each of the cDNA constructs with T7 polymerase and capped with 5′7-methylguanosine by use of the mMESSAGE mMACHINE (Ambion Inc.). Approximately 50 ng of the various cRNAs was injected into defolliculated stage V and VI *Xenopus laevis* oocytes and transport was assayed 3 to 4 days later.

Transport Measurements. Uptake of D-[^{3}H]aspartate was performed essentially as described (32), after pretreatment with DTT or CuPh, as detailed in the *SI Materials and Methods*.

Note Added in Proof. A 3.5 Å-resolution X-ray crystallographic structure of GltPh in which HP2 and TM2 are cross-linked by Hg^{2+} has recently been reported (34). This structure agrees remarkably well with our prediction of the major conformational change that occurs during transport, providing convincing evidence that inverted-topology structural repeats are responsible for the creation of two symmetry-related states in transporter proteins. Furthermore, our data for EAAC1 demonstrates that the predicted and observed conformational changes in the bacterial transporter also occur during transport of neuronal glutamate.

ACKNOWLEDGMENTS. We thank J. Faraldo-Gómez for valuable suggestions. This work was supported by SFB-807 from the Deutsche Forschungsgesellschaft (to L.R.F), the National Institute of Neurological Disorders and Stroke through National Institutes of Health Grant NS16708, and US–Israel Binational Science Foundation Grant 2007051 (to B.I.K.).

1. Zerangue N, Kavanaugh MP (1996) Flux coupling in a neuronal glutamate transporter. *Nature* 383:634–637.
2. Levy LM, Warr O, Attwell D (1998) Stoichiometry of the glial glutamate transporter GLT-1 expressed inducibly in a chinese hamster ovary cell line selected for low endogenous Na^+-dependent glutamate uptake. *J Neurosci* 18:9620–9628.
3. Kanner BI, Bendahan A (1982) Binding order of substrates to the sodium and potassium ion coupled L-glutamic acid transporter from rat brain. *Biochem* 21:6327–6330.
4. Pines G, Kanner BI (1990) Counterflow of L-glutamate in plasma membrane vesicles and reconstituted preparations from rat brain. *Biochem* 29:11209–11214.
5. Kavanaugh MP, Bendahan A, Zerangue N, Zhang Y, Kanner BI (1997) Mutation of an amino acid residue influencing potassium coupling in the glutamate transporter GLT-1 induces obligate exchange. *J Biol Chem* 272:1703–1708.
6. Yernool D, Boudker O, Jin Y, Gouaux E (2004) Structure of a glutamate transporter homologue from *Pyrococcus horikoshii. Nature* 431:811–818.
7. Boudker O, Ryan RM, Yernool D, Shimamoto K, Gouaux E (2007) Coupling substrate and ion binding to extracellular gate of a sodium-dependent aspartate transporter. *Nature* 445:387–393.
8. Kanner BI (2007) Gate movements in glutamate transporters. *Chem Biol* 2:163–166.
9. Jardetzky O (1966) Simple allosteric model for membrane pumps. *Nature* 211:969–970.
10. Forrest LR, et al. (2008) A mechanism for alternating access in neurotransmitter transporters. *Proc Natl Acad Sci USA* 105:10338–10343.
11. Faham S, et al. (2008) The crystal structure of a sodium galactose transporter reveals mechanistic insights into Na^+/sugar symport. *Science* 321:810–814.
12. Shlaifer I, Kanner BI (2007) Conformationally sensitive reactivity to permeant sulfhydryl reagents of cysteine residues engineered into helical hairpin 1 of the glutamate transporter GLT-1. *Mol Pharmacol* 71:1341–1348.
13. Krishnamurthy H, Piscitelli CL, Gouaux E (2009) Unlocking the molecular secrets of sodium-coupled transporters. *Nature* 459:347–355.
14. Groeneveld M, Slotboom D-J (2007) Rigidity of the subunit interfaces of the trimeric glutamate transporter GltT during translocation. *J Mol Biol* 372:565–570.
15. Ryan RM, Mitrovic AD, Vandenberg RJ (2004) The chloride permeation pathway of a glutamate transporter and its proximity to the glutamate translocation pathway. *J Biol Chem* 279:20742–20751.
16. Brocke L, Bendahan A, Grunewald M, Kanner BI (2002) Proximity of two oppositely oriented reentrant loops in the glutamate transporter GLT-1 identified by paired cysteine mutagenesis. *J Biol Chem* 277:3985–3992.
17. Zomot E, Zhou YG, Kanner BI (2005) Proximity of transmembrane domains 1 and 3 of the gamma-aminobutyric acid transporter GAT-1 inferred from paired cysteine mutagenesis. *J Biol Chem* 280:25512–25516.
18. Leighton BH, Seal RP, Watts SD, Skyba MO, Amara SG (2006) Structural rearrangements at the translocation pore of the human glutamate transporter, EAAT1. *J Biol Chem* 281:29788–29796.
19. Gu Y, Shrivastava IH, Amara SG, Bahar I (2009) Molecular simulations elucidate the substrate translocation pathway in a glutamate transporter. *Proc Natl Acad Sci USA* 106:2589–2594.
20. Mim C, Tao Z, Grewer C (2007) Two conformational changes are associated with glutamate translocation by the glutamate transporter EAAC1. *Biochem* 46:9007–9018.
21. Koch HP, Larsson HP (2005) Small-scale molecular motions accomplish glutamate uptake in human glutamate transporters. *J Neurosci* 25:1730–1736.
22. Qu S, Kanner BI (2008) Substrates and non-transportable analogues induce structural rearrangements at the extracellular entrance of the glial glutamate transporter GLT-1/EAAT2. *J Biol Chem* 283:26391–26400.
23. Huang Z, Tajkhorshid E (2008) Dynamics of the extracellular gate and ion-substrate coupling in the glutamate transporter. *Biophys J* 95:2292–2300.
24. Shrivastava IH, Jiang J, Amara SG, Bahar I (2008) Time-resolved mechanism of extracellular gate opening and substrate binding in a glutamate transporter. *J Biol Chem* 283:28680–28690.
25. Grunewald M, Kanner B (1995) Conformational changes monitored on the glutamate transporter GLT-1 indicate the existence of two neurotransmitter-bound states. *J Biol Chem* 270:17017–17024.
26. Thompson JD, Higgins DG, Gibson TJ (1994) CLUSTAL W: improving the sensitivity of progressive multiple sequence alignment through sequence weighting, position-specific gap penalties and weight matrix choice. *Nucl Acids Res* 22:4673–4680.
27. Šali A, Blundell TL (1993) Comparative protein modelling by satisfaction of spatial restraints. *J Mol Biol* 234:779–815.
28. Kanai Y, Hediger MA (1992) Primary structure and functional characterization of a high-affinity glutamate transporter. *Nature* 360:467–471.
29. Borre L, Kanner BI (2004) Arginine 445 controls the coupling between glutamate and cations in the neuronal transporter EAAC-1. *J Biol Chem* 279:2513–2519.
30. Pines G, Zhang Y, Kanner BI (1995) Glutamate 404 is involved in the substrate discrimination of GLT-1, a (Na^+ + K^+)-coupled glutamate transporter from rat brain. *J Biol Chem* 270:17093–17097.
31. Kunkel TA, Roberts JD, Zakour RA (1987) Rapid and efficient site-specific mutagenesis without phenotypic selection. *Methods Enzymol* 154:367–382.
32. Bendahan A, Armon A, Madani N, Kavanaugh MP, Kanner BI (2000) Arginine 447 plays a pivotal role in substrate interactions in a neuronal glutamate transporter. *J Biol Chem* 275:37436–37442.
33. DeLano W (2008) *The PyMOL Molecular Graphics System* (DeLano Scientific LLC, Palo Alto, CA).
34. Reyes N, Ginter C, Boudker O (2009) Transport mechanism of a bacterial homologue of glutamate transporters. *Nature*, 10.1038/nature08616.